JCI insight

RESEARCH ARTICLE

Platelet integrin α6β1 controls lung metastasis through direct binding to cancer cell–derived ADAM9

Elmina Mammadova-Bach,[1] Paola Zigrino,[2] Camille Brucker,[1] Catherine Bourdon,[1] Monique Freund,[1] Adèle De Arcangelis,[3] Scott I. Abrams,[4] Gertaud Orend,[5] Christian Gachet,[1] and Pierre Henri Mangin[1]

[1]UMR-S949, INSERM, Etablissement Français du Sang-Alsace, Université de Strasbourg, Strasbourg, France. Fédération de Médecine Translationnelle de Strasbourg, Strasbourg, France. [2]Department of Dermatology and Venerology, University of Cologne, Cologne, Germany. [3]U964, INSERM, UMR 7104, CNRS, Université de Strasbourg, Institut de Génétique et de Biologie Moléculaire et Cellulaire, Illkirch, Strasbourg, France. [4]Department of Immunology, Roswell Park Cancer Institute, Buffalo, New York, USA. [5]INSERM U1109, The Microenvironmental Niche in Tumorigenesis and Targeted Therapy, Université de Strasbourg, Fédération de Médecine Translationnelle de Strasbourg, LabEx Medalis, Strasbourg, France.

Metastatic dissemination of cancer cells, which accounts for 90% of cancer mortality, is the ultimate hallmark of malignancy. Growing evidence suggests that blood platelets have a predominant role in tumor metastasis; however, the molecular mechanisms involved remain elusive. Here, we demonstrate that genetic deficiency of integrin α6β1 on platelets markedly decreases experimental and spontaneous lung metastasis. In vitro and in vivo assays reveal that human and mouse platelet α6β1 supports platelet adhesion to various types of cancer cells. Using a knockdown approach, we identified ADAM9 as the major counter receptor of α6β1 on both human and mouse tumor cells. Static and flow-based adhesion assays of platelets binding to DC-9, a recombinant protein covering the disintegrin-cysteine domain of ADAM9, demonstrated that this receptor directly binds to platelet α6β1. In vivo studies showed that the interplay between platelet α6β1 and tumor cell–expressed ADAM9 promotes efficient lung metastasis. The integrin α6β1–dependent platelet-tumor cell interaction induces platelet activation and favors the extravasation process of tumor cells. Finally, we demonstrate that a pharmacological approach targeting α6β1 efficiently impairs tumor metastasis through a platelet-dependent mechanism. Our study reveals a mechanism by which platelets promote tumor metastasis and suggests that integrin α6β1 represents a promising target for antimetastatic therapies.

Introduction

Metastasis is the leading cause of cancer-related death and represents a major challenge in patient care. To metastasize, a tumor cell must undergo various steps of cancer progression, including detachment from the primary tumor, intravasation into the vascular system directly or through lymph nodes, survival in the circulation, arrest on endothelial cells, and finally extravasation, survival, and proliferation in distant organs (1, 2). Metastasis is a highly inefficient process, as less than 0.1% of tumor cells which penetrate the circulation end up forming metastatic colonies (3, 4). The molecular events driving metastasis, notably those occurring within the bloodstream and related to their physical and functional interaction with circulating blood cells, remain incompletely understood.

Once they enter the bloodstream, tumor cells come in the vicinity of circulating cells and rapidly bind to platelets (5). This physical interaction might allow platelets to participate in the metastatic dissemination by regulating various tumor cell functions (5, 6). Platelets were proposed to form a physical shield around tumor cells protecting them from shear stress and cytotoxic effects of natural killers (7, 8). Moreover, platelets were proposed to promote epithelial-mesenchymal transition of tumor cells through TGF-β and NF-κB signaling, thus promoting tumor metastasis (9). They could also support tumor cell attachment to the endothelium (10–12) and promote their extravasation by increasing endothelial permeability (13).

Tumor cells interact with their environment through a variety of transmembrane proteins, including integrins, selectins, cadherins, and other intercellular adhesion molecules that not only support cell-cell

Conflict of interest: The authors have declared that no conflict of interest exists.

Submitted: May 9, 2016
Accepted: August 2, 2016
Published: September 8, 2016

Reference information:
JCI Insight. 2016;1(14):e88245.
doi:10.1172/jci.insight.88245.

interactions, but also mediate tumor progression and metastasis (1, 14–16). Concerning platelets, specific surface receptors, such as C-type lectin-like receptor 2 (CLEC-2) (17), and the integrin αIIbβ3 (18–20) mediate interactions between platelets and tumor cells. Platelets also express other integrins, such as αvβ3 and 3 β1-containing integrins, namely α2β1, α5β1, and α6β1. Using mice with a genetic deletion of α6β1 in platelets, we previously reported that this integrin supports platelet adhesion and activation of vascular laminins and promotes experimental thrombus formation, while playing no major role in hemostatic functions (21). To date, the role of the platelet β1 integrins, notably α6β1, in physical and functional interactions with tumor cells and in metastatic dissemination is completely unknown.

Integrin α6β1, which is expressed on cancer and endothelial cells, has been described to favor tumor angiogenesis, invasiveness, and cancer progression (22–27). Besides laminins, this integrin has also been reported to bind ADAM9/meltrin-γ, a member of the a disintegrin and metalloproteinase (ADAM) family of proteins (28, 29). The ADAM family of membrane-anchored proteins contains a number of characteristic domains, including a signal sequence followed by a prodomain, a metalloproteinase domain, a disintegrin-like domain, and a short cytoplasmic tail. Members of the ADAM family have been implicated in a number of important cellular processes, including cell-cell and cell-matrix interactions, cell fusion, and cell signaling (30). Although studies have often focused on the proteolytic activity of members of this family, there is increasing evidence that they play a role in cell adhesion through direct interaction with integrins. ADAM9 is a widely expressed non–Arg-Gly-Asp–containing molecule, which has been shown to bind to αvβ5 on myeloma cells, α3β1 on keratinocytes, and α6β1 on fibroblasts (28, 29, 31–34). These studies raise the possibility that ADAM9 could mediate cell-platelet interactions to regulate dissemination of cancer cells.

The proposed role of platelet adhesion receptors in metastatic dissemination and the involvement of integrin receptors in several hallmarks of tumor cells prompted us to investigate whether platelet integrin α6β1 participates in tumor metastasis. In this study, we demonstrate that platelets promote spontaneous and experimental lung metastasis through an interaction between platelet integrin α6β1 and ADAM9 expressed on tumor cells. Our findings reveal that platelet integrin α6β1 and its counter receptor ADAM9 on tumor cells may represent new therapeutic targets to prevent metastasis.

Results

Genetic deficiency of α6β1 integrin on platelets leads to decreased tumor metastasis in mice. Spontaneous transplant models of metastasis encompass several steps of the tumor process, from primary tumor growth to subsequent metastasis. We used breast cancer cells (AT-3 cells) derived from primary tumors of mammary tumor virus–driven polyoma middle T (MMTV-PyMT) transgenic mice, which, upon orthotopic injection in the mammary fat pad of C57BL/6 mice, developed primary tumors that metastasized into the lungs (Figure 1A). Grafting of these cells led to the growth of mammary tumors with a similar kinetic in platelet-specific knockout of α6 *(PF4-Cre-α6$^{-/-}$)* or β1 (*PF4-Cre-β1$^{-/-}$*) integrin mice as compared with controls (Figure 1, B and C). In contrast, the number of spontaneous lung metastases was reduced by 1.9-fold and 2.1-fold in *PF4-Cre-α6$^{-/-}$* and *PF4-Cre-β1$^{-/-}$* mice when compared with controls, highlighting a role of platelet α6β1 in tumor metastasis (Figure 1, D–G). This was further confirmed when AT-3 tumor cells were injected directly into the tail vein (Figure 1H), which also resulted in a significant decrease in tumor cell colonization to the lungs in *PF4-Cre-α6$^{-/-}$* (Figure 1I) and *PF4-Cre-β1$^{-/-}$* (Figure 1J) mice when compared with controls. Moreover, similar results were obtained in 3 distinct experimental metastasis models based on i.v. injection of B16F10 melanoma cells (Figure 1, H, K, and L), MC38 colon carcinoma cells (Supplemental Figure 1A; supplemental material available online with this article; doi:10.1172/jci.insight.88245DS1), and E0771 medullary mammary adenocarcinoma cells (Supplemental Figure 1B), all of which resulted in a marked reduction in pulmonary metastases in *PF4-Cre-α6$^{-/-}$* mice as compared with controls. Collectively, these data support a major role for platelet integrin α6β1 in tumor metastasis.

Integrin α6β1 mediates direct interaction of platelets with tumor cells. Distant metastases mainly occur through hematogenous dissemination via the blood circulation, and platelets were proposed to be the first blood cells to interact with tumor cells (5). To determine whether integrin α6β1 supports platelet-tumor cell interaction, washed fluorescently labeled platelets were allowed to adhere to tumor cells under static conditions. As shown in Figure 2, A and B, deficiency of α6β1 resulted in a 2.6-, 2.8-, and 1.5-fold reduction in washed mouse platelet recruitment to AT-3 breast cancer, MC38 colon carcinoma, and B16F10 melanoma cells as compared with controls. Similar results were obtained with washed human platelets in which the α6-blocking antibody, GoH3, reduced platelet adhesion to human breast and colon cancer cells (MDA-MB-231,

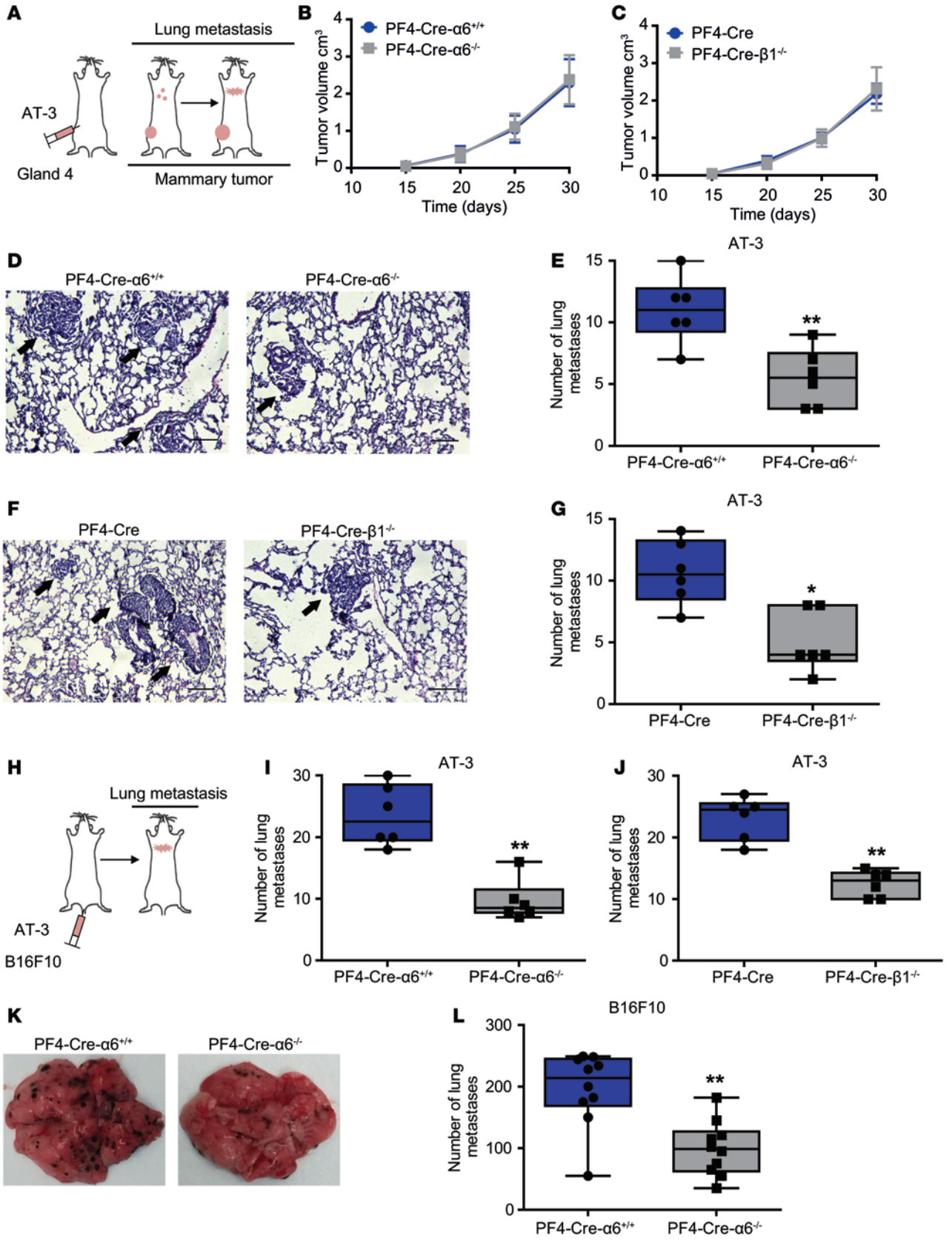

Figure 1. Lack of platelet integrin α6β1 inhibits tumor metastasis. (**A**) Schematic of a mouse orthotopic metastasis assay. AT-3 tumor cells were injected into the fourth mammary fat pad of *PF4-Cre-α6*$^{-/-}$, *PF4-Cre-β1*$^{-/-}$, and control mice, and the volume of primary tumor in the mammary fat pad and the number of lung metastasis were determined. (**B** and **C**) Kinetic of primary tumor growth in (**B**) *PF4-Cre-α6*$^{+/+}$ and *PF4-Cre-α6*$^{-/-}$ mice and (**C**) *PF4-Cre* and *PF4-Cre-β1*$^{-/-}$ mice. Six mice per each group were used. Error bars represent S.E.M. (**D** and **F**) Representative H&E-stained sections

obtained from lungs of AT-3–injected (**D**) *PF4-Cre-α6*$^{+/+}$ and *PF4-Cre-α6*$^{-/-}$ and (**F**) *PF4-Cre* and *PF4-Cre-β1*$^{-/-}$ mice. Black arrows indicate metastatic nodules. Scale bar: 200 μm. (**H**) Schematic of a lung colonization assay following i.v. injection of (**I** and **J**) AT-3 or (**K** and **L**) B16F10 tumor cells in indicated mice. Numbers of metastatic foci in lung tissues of AT-3–injected (**E** and **I**) *PF4-Cre-α6*$^{+/+}$ and *PF4-Cre-α6*$^{-/-}$ mice and (**G** and **J**) *PF4-Cre* and *PF4-Cre-β1*$^{-/-}$ mice. *$P < 0.05$, **$P < 0.01$, Mann-Whitney test. (**K**) Representative photographs obtained from lungs of B16F10-injected *PF4-Cre-α6*$^{+/+}$ and *PF4-Cre-α6*$^{-/-}$ mice. (**L**) Numbers of metastatic nodules on the surface of B16F10-injected *PF4-Cre-α6*$^{+/+}$ and *PF4-Cre-α6*$^{-/-}$ mice. **$P < 0.01$, Student's *t* test. (**E**, **G**, **I**, **J**, and **L**) Each point represents an individual mouse. Box-and-whisker plots were used to graphically represent the median (line within box), upper and lower quartile (bounds of box), and maximum and minimum values (bars).

SKRB3, and LoVo by 1.7-, 1.9-, and 3-fold) compared with an isotype control (Figure 2C). A blocking anti-β1 antibody reduced to a similar level platelet recruitment to MDA-MB-231, SKRB3, and LoVo cells (Figure 2C). We next aimed to confirm the role of α6β1 in platelet-tumor cell interaction in vivo. Therefore, we used *c-mpl*$^{-/-}$ mice (35), which present the advantage of having a low platelet count (~300,000 platelet/μl), and injected them with RAM.1 antibody–labeled washed mouse platelets together with CFSE-labeled AT-3 cells (Figure 2D). Immunofluorescence analysis of lungs collected 2 hours after injection revealed that the number of tumor cells surrounded with platelets was reduced 2.3-fold in mice transfused with *PF4-Cre-α6*$^{-/-}$ platelets compared with those transfused with *PF4-Cre-α6*$^{+/+}$ platelets (Figure 2, E and F). We next assessed the impact of defective α6β1-dependent platelet-tumor cell interaction on experimental metastasis. We first showed that AT-3 cell–driven lung metastasis was markedly impaired in thrombocytopenic *c-mpl*$^{-/-}$ mice as compared with WT mice, confirming the importance of the platelet count in tumor cell colonization to the lungs (Figure 2G). Interestingly, we found that transfusion of *PF4-Cre-α6*$^{+/+}$ platelets, but not *PF4-Cre-α6*$^{-/-}$ platelets, in *c-mpl*$^{-/-}$ mice partially restored lung metastasis (Figure 2G). These results demonstrate that α6β1 ensures platelet-tumor cell interaction, thereby promoting lung metastasis.

Integrin α6β1 supports platelet-tumor cell interaction through direct binding to ADAM9. We next decided to identify the counter receptor of platelet α6β1 on tumor cells. We hypothesized that this receptor could be ADAM9, because this membrane-anchored molecule was reported to bind α6β1 integrin through its disintegrin domain (28, 29, 31). ADAM9 is expressed in several tumor cells (30), including cell lines employed in our studies (Figure 3A and Supplemental Figure 2). To assess whether ADAM9 is a receptor of platelet α6β1 integrin on tumor cells, we generated AT-3 and MC38 cells knocked down for ADAM9 expression by using a shRNA lentiviral approach. All sh ADAM9 clones presented a marked reduction in ADAM9 expression in both transcriptional (Figure 3A) and protein levels (Figure 3B), without downregulation of other ADAM family members (Supplemental Figure 3) and additional proteolytic enzymes (Supplemental Figure 4). We first provided evidence for a role of ADAM9 in platelet-tumor cell interaction, as evidenced by a 1.8- (sh1) and 2- (sh2) as well as a 1.6- (sh1) and 1.8-fold (sh2) reduction in interaction of washed *PF4-Cre-α6*$^{+/+}$ platelets with ADAM9 knocked down AT-3 and MC38, respectively (Figure 3, C and D). Interestingly, the level of *PF4-Cre-α6*$^{+/+}$ platelet adhesion to ADAM9-deficient AT-3 and MC38 cells was similar to that of *PF4-Cre-α6*$^{-/-}$ platelet recruitment to control cells. Moreover, no additive inhibitory effect was observed when *PF4-Cre-α6*$^{-/-}$ platelets were added to ADAM9-deficient tumor cells, suggesting that the platelet-tumor cell interaction results from an interplay between α6β1 and ADAM9 (Figure 3, C and D). Similar results were obtained with ADAM9 knocked down MDA-MB-231 human breast cancer cells, which presented a marked reduction in the adhesion of human platelets (Supplemental Figure 5). To investigate whether adhesion of platelets to tumor cells was mediated by a direct interaction between integrin α6β1 and ADAM9, we allowed *PF4-Cre-α6*$^{-/-}$ and *PF4-Cre-β1*$^{-/-}$ platelets to adhere to a recombinant protein consisting of the disintegrin-like and the cysteine-rich domain of ADAM9 (DC-9) (33). Adhesion of *PF4-Cre-α6*$^{-/-}$ and *PF4-Cre-β1*$^{-/-}$ platelets to DC-9 under static conditions was significantly decreased by 4- and 6-fold, respectively, compared with controls (Figure 3, E and F). A similar inhibition in adhesion of α6β1-deficient platelets was observed when anticoagulated whole blood was perfused over DC-9 at 300 s^{-1} (Figure 3, G and H). In summary, these data indicate that ADAM9 present at the surface of tumor cells is a counter receptor of integrin α6β1, supporting platelet adhesion to tumor cells.

The interplay between platelet integrin α6β1 and tumor cell–derived ADAM9 controls lung metastasis. To assess the functional relevance of α6β1-ADAM9 interplay in metastasis, control or ADAM9-deficient AT-3 cells were injected into the mammary fad pads of *PF4-Cre-α6*$^{+/+}$ or *PF4-Cre-α6*$^{-/-}$ mice. Volumes of primary tumors were very similar at the various time points studied, regardless of the experimental condition, indicating that neither platelet α6β1, nor tumor cell–expressed ADAM9 are critical for the primary tumor growth (Figure 4A). In *PF4-Cre-α6*$^{+/+}$ mice, administration of ADAM9-deficient AT-3 cells (sh1 and sh2)

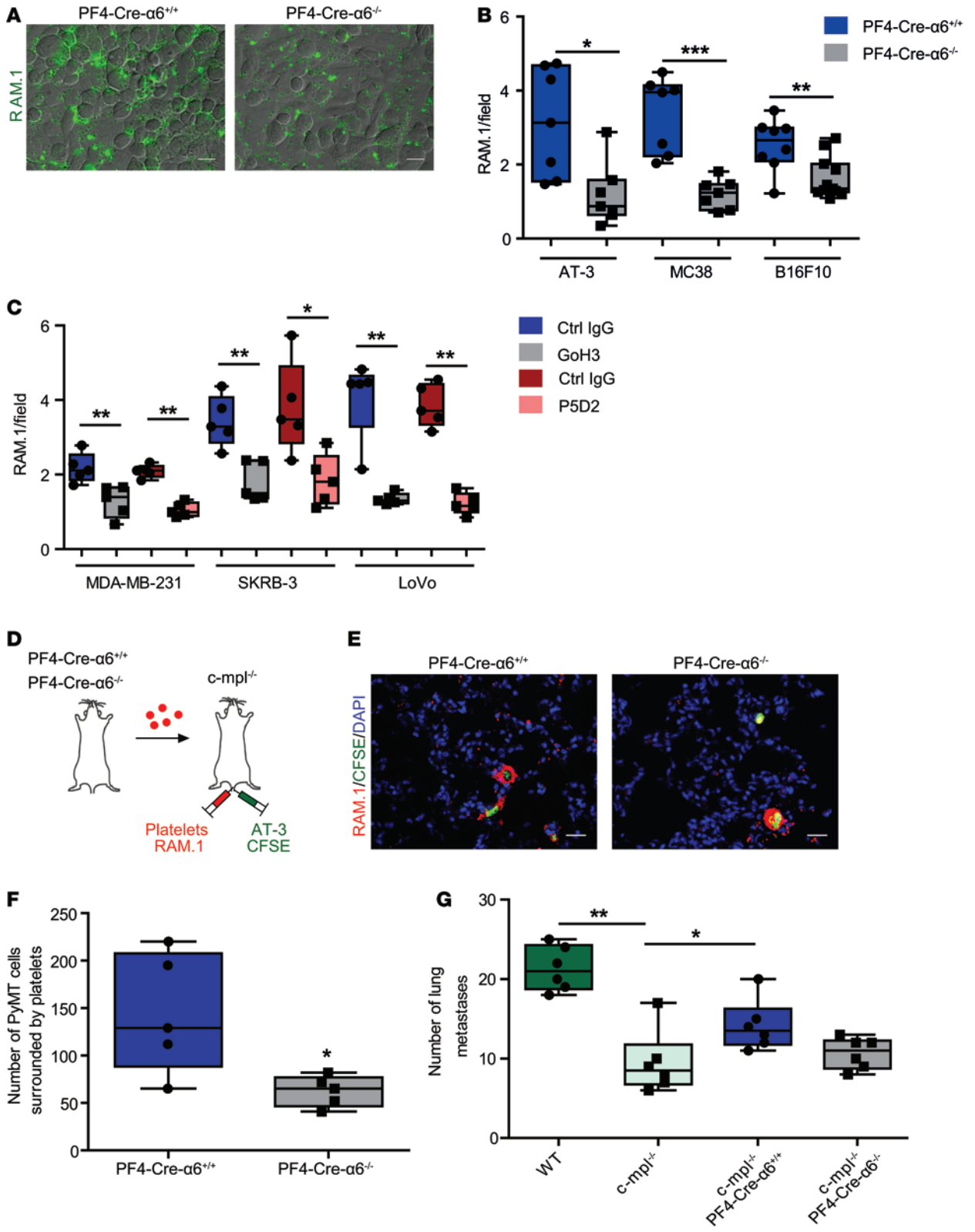

Figure 2. Platelet integrin α6β1 deficiency or blockade impairs platelet and tumor cell interaction. Platelet adhesion to tumor cells was quantified based on the fluorescence detection of RAM.1-labeled platelets, as described in Methods. (**A**) Representative epifluorescence microcopy images of RAM.1-Alexa 488–labeled mouse *PF4-Cre-α6*$^{+/+}$ and *PF4-Cre-α6*$^{-/-}$ platelets (green) adhering to AT-3 tumor cells. Scale bar: 50 μm. (**B** and **C**) Quantification of the fluorescent signal corresponding to the amount of platelets allowed to adhere to tumor cells. (**B**) Washed *PF4-Cre-α6*$^{+/+}$ or *PF4-Cre-α6*$^{-/-}$ mouse platelets were allowed to adhere on AT-3 breast cancer, MC38 colon carcinoma, and B16F10 melanoma cells. (**C**) Washed human platelets were treated with an irrelevant IgG (control) or blocking antibodies against α6 (GoH3) or β1 (P5D2) integrin (10 μg/ml) and cultured on MDA-MB-231, SKRB-3 breast, and LoVo colon cancer cells. *$P < 0.05$, **$P < 0.01$, ***$P < 0.001$, Mann-Whitney test. (**D**) Experimental design. *c-mpl*$^{-/-}$ mice were injected with

RAM.1-cy3–labeled *PF4-Cre-α6*$^{+/+}$ or *PF4-Cre-α6*$^{-/-}$ platelets (red) and CFSE-labeled AT-3 tumor cells (green). (**E**) Two hours after injection, mice were euthanized and lungs were collected, and the colocalization of AT-3 tumor cells with platelets was determined by fluorescence microscopy. Nuclei were stained with DAPI (blue). Scale bar: 20 μm. (**F**) Quantification of the number of tumor cells surrounded by platelets. *P < 0.05, Mann-Whitney test. (**G**) WT or *c-mpl*$^{-/-}$ mice were transfused or not with *PF4-Cre-α6*$^{+/+}$ and *PF4-Cre-α6*$^{-/-}$ platelets. In parallel, these mice were also injected with AT-3 cells through a different tail vein. Experimental lung metastasis was determined 20 days of after injection. Numbers of metastatic foci in lung tissues of AT-3–injected WT or *c-mpl*$^{-/-}$ mice. *P < 0.05, **P < 0.01, Mann-Whitney test. Each point represents (**B**, **F**, and **G**) an individual mouse or (**C**) healthy human donor. (**B**, **C**, **F**, and **G**) Box-and-whisker plots were used to graphically represent the median (line within box), upper and lower quartile (bounds of box), and maximum and minimum values (bars). *P < 0.05, **P < 0.01, ***P < 0.001.

led to an approximately 2-fold reduction in the number of lung metastases compared with control cells (Figure 4B). ADAM9 knockdown caused a similar impairment in lung colonization of AT-3 or MC38 tumor cells following inoculation via the tail vein (Figure 4, C and D). Of note, in both experimental and spontaneous lung metastasis models, ADAM9 deficiency did not cause an additional decrease in lung metastasis in *PF4-Cre-α6*$^{-/-}$ mice, and no further inhibition was achieved when both α6β1 and ADAM9 were lacking, suggesting that the α6β1-ADAM9 interplay mediates metastasis (Figure 4, B–D). To provide further evidence, *PF4-Cre-α6*$^{+/+}$ and *PF4-Cre-α6*$^{-/-}$ washed platelets were transfused into *PF4-Cre-α6*$^{-/-}$ mice together with control or AT-3–deficient ADAM9 cells (Figure 4E). As shown in Figure 4E, transfusion of WT, but not α6β1-deficient, platelets partially rescued AT-3 cell–induced metastasis in *PF4-Cre-α6*$^{-/-}$ mice. In contrast, transfusion of WT platelets failed to restore metastasis when ADAM9-deficient AT-3 cells were injected into *PF4-Cre-α6*$^{-/-}$ mice (Figure 4E). Thus, our results suggest that platelet α6β1 integrin enhances lung metastasis through direct interaction with ADAM9 expressed on tumor cells.

Platelet α6β1 binding to tumor cell ADAM9 promotes platelet activation, granule secretion, and tumor cell extravasation. To get insight into the mechanism by which platelet α6β1 promotes metastasis through an interplay with ADAM9, we evaluated the impact of its absence on DC9-mediated platelet activation. We found that deficiency of α6β1 significantly decreased DC-9–induced filopodia extension of adherent platelets (Figure 5, A and B). We also observed that *PF4-Cre-α6*$^{-/-}$ platelets adherent to DC-9 presented a significant reduction of P-selectin exposure, a recognized marker of α-granule secretion, when compared with controls (Figure 5, C and D). In agreement, we could show that *PF4-Cre-α6*$^{-/-}$ platelets adherent to AT-3 tumor cells, exposed less P-selectin at their surface, suggesting that α6β1 is involved in tumor cell–induced platelet activation (Figure 5, E and F). Altogether, these results suggest that direct interaction of α6β1 with ADAM9 promotes platelet activation and granule secretion. Recent studies reported that tumor cell–activated platelets promote extravasation of circulating tumor cells, thereby enhancing their metastatic potential (13). Thus, we hypothesized that the interplay between platelet integrin α6β1 and ADAM9 could favor tumor cell extravasation. To evaluate this hypothesis, control and ADAM9-silenced AT-3 cells were allowed to migrate through an endothelial cell layer–coated Transwell insert alone or in presence of *PF4-Cre-α6*$^{+/+}$ or *PF4-Cre-α6*$^{-/-}$ platelets. We first observed that addition of washed WT platelets enhanced transendothelial migration of AT-3 cells by 2.7-fold compared with controls (Figure 5G). In contrast, combining *PF4-Cre-α6*$^{-/-}$ platelets with control tumor cells, or *PF4-Cre-α6*$^{+/+}$ platelets with ADAM9-deficient AT-3 cells, failed to increase transendothelial migration (Figure 5G). This result suggests that the interplay between platelet integrin α6β1 and ADAM9 favors tumor cell extravasation in vitro. To determine whether platelet integrin α6β1 has a similar effect in vivo, CFSE-labeled AT-3 cells were i.v. injected into *PF4-Cre-α6*$^{+/+}$ and *PF4-Cre-α6*$^{-/-}$ mice. While the number of tumor cells present in the lungs was normal 6 hours after injection (Supplemental Figure 6), a smaller proportion of them were localized in the extravascular compartment in *PF4-Cre-α6*$^{-/-}$ mice compared with controls (Figure 5, H and I). Collectively, these data suggest that platelet α6β1 and tumor ADAM9 cooperate to promote platelet activation and granule secretion and to ensure efficient tumor cell extravasation, thereby promoting tumor metastasis.

Pharmacological targeting of integrin α6β1 reduces tumor metastasis. To explore the antimetastatic potential of a pharmacological strategy aiming to target α6β1 integrin (Figure 6A), mice inoculated with AT-3 (Figure 6B) or B16F10 (Figure 6, C and D) tumor cells were treated by tail vein injection together with a control or the anti–α6-blocking antibody GoH3. We first demonstrated that administration of 2 mg/kg of GoH3 did not induce a thrombocytopenia (Figure 6A) and had no impact on the level of circulating red blood cells, white blood cells, and hemoglobin (Supplemental Figure 7). Importantly, GoH3 treatment efficiently inhibited lung metastasis mediated by both tumor cell lines in control mice (Figure 6, B and C). Its specificity is evidenced by the finding that GoH3 displayed no effect in *PF4-Cre-α6*$^{-/-}$ mice (Figure 6, B and C). Interestingly, administration of GoH3 at day 5 after injection of tumor cells did not inhibit anymore tumor

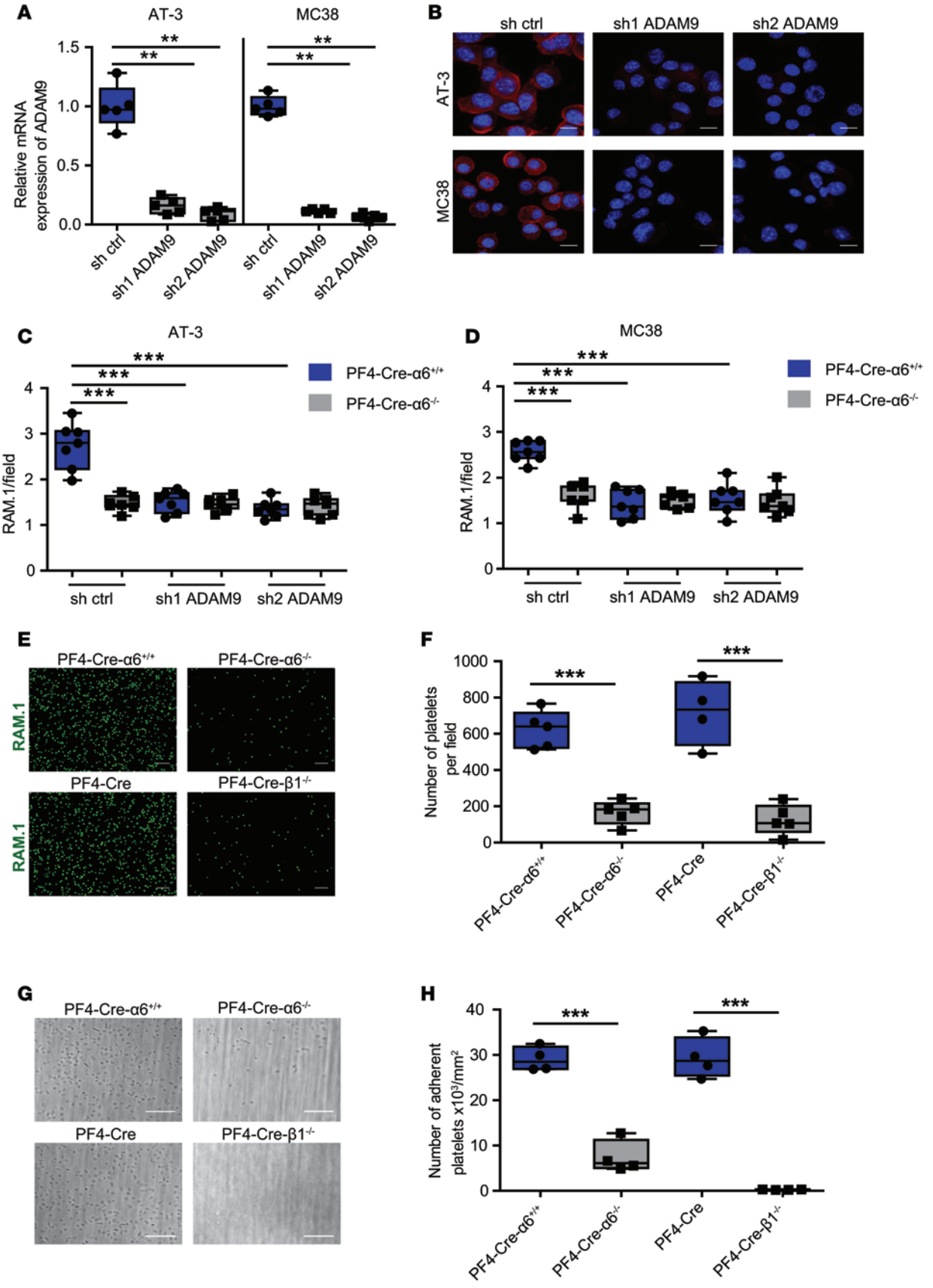
A
AT-3
MC38
Relative mRNA expression of ADAM9
sh ctrl
sh1 ADAM9
sh2 ADAM9
B
sh ctrl
sh1 ADAM9
sh2 ADAM9
AT-3
MC38
C
AT-3
PF4-Cre-α6+/+
PF4-Cre-α6-/-
RAM.1/field
D
MC38
E
PF4-Cre-α6+/+
PF4-Cre-α6-/-
PF4-Cre
PF4-Cre-β1-/-
RAM.1
F
Number of platelets per field
G
H
Number of adherent platelets x10³/mm²

Figure 3. ADAM9 expressed on tumor cells supports integrin α6β1–dependent platelet adhesion through its disintegrin-cysteine rich domain. (**A** and **B**) Downregulation of ADAM9 expression in AT-3 and MC38 cells with two distinct ADAM9 shRNAs. (**A**) ADAM9 mRNA expression was determined by qRT-PCR and normalized with mRNA level of GAPDH. $^{**}P < 0.01$, Mann-Whitney test. Each point represents a separate experiment. (**B**) Representative immunofluorescence images of AT-3 and MC38 cells knocked down or not for ADAM9, with an anti-ADAM9 antibody (IF: in red). Nuclei were stained with DAPI (blue). Scale bar: 50 μm. (**C** and **D**) Quantification of the fluorescent signal corresponding to the amount of *PF4-Cre-α6*$^{+/+}$ and *PF4-Cre-α6*$^{-/-}$ mouse platelets adhered to (**C**) AT-3 and (**D**) MC38 control or ADAM9-silenced (sh1 and sh2) cancer cells. $^{***}P < 0.001$, Mann-Whitney test. Each point represents an individual mouse. (**E** and **G**) Representative (**E**) immunofluorescence and (**G**) differential interference contrast microscopy images of *PF4-Cre-α6*$^{+/+}$ and *PF4-Cre-α6*$^{-/-}$ mouse platelets adhering to recombinant DC-9 ADAM9 under (**E**) static and (**G**) flow conditions, respectively. Scale bar: 20 μm. (**E**) Washed *PF4-Cre-α6*$^{+/+}$, *PF4-Cre-α6*$^{-/-}$, *PF4-Cre*, and *PF4-Cre-β1*$^{-/-}$ mouse platelets were allowed to adhere to glass coverslips coated with 500 μg/ml DC-9 ADAM9. After 30 minutes, adherent cells were fixed, stained with the RAM.1 antibody (RAM.1), and observed by epifluorescent microscopy. (**G**) Hirudinated *PF4-Cre-α6*$^{+/+}$, *PF4-Cre-α6*$^{-/-}$, *PF4-Cre*, and *PF4-Cre-β1*$^{-/-}$ mouse whole blood was perfused through DC-9 (500 μg/ml) coated microcapillaries at 300 s^{-1} and monitored for 3 minutes. *PF4-Cre-α6*$^{+/+}$, *PF4-Cre-α6*$^{-/-}$, *PF4-Cre*, and *PF4-Cre-β1*$^{-/-}$ mouse platelet adhesion was observed by real-time video microscopy. (**F** and **H**) Quantification of the number of adherent platelets under (**F**) static and (**H**) flow condition. $^{***}P < 0.001$, Mann-Whitney test. Each point represents an individual mouse. Box-and-whisker plots were used to graphically represent the median (line within box), upper and lower quartile (bounds of box), and maximum and minimum values (bars).

metastasis, suggesting that this integrin plays a role in early stages of the metastatic process (Figure 6D). These data further confirmed the requirement of platelet integrin α6β1 for efficient metastasis and suggest that blockade of this receptor may represent a powerful strategy to prevent tumor cell dissemination at early stages of metastasis.

Discussion

Over the last few decades, although numerous potential mechanisms through which platelets mediate tumor metastasis were proposed, the molecular events driving direct platelet-tumor cell interplay still remain incompletely understood. In the present report, by employing a megakaryocyte-restricted knockout strategy, we highlighted a major role for integrin α6β1 in supporting direct platelet binding to tumor cells. We identified ADAM9 as being the counter receptor of platelet α6β1 on tumor cells. We also provided evidence that the interaction of α6β1 with ADAM9 promotes platelet activation and subsequent tumor cell extravasation, thereby favoring lung metastasis associated notably to breast cancer.

A major highlight of our study relies on the identification of an important contribution of platelet integrin α6β1 to tumor metastasis. Evidence was derived, not only from a pharmacological approach based on a blocking anti–integrin α6 antibody, but also from mice that were specifically knocked out for integrin α6 in the megakaryocytic lineage. Moreover, we showed that transfusion of WT, but not α6-deficient, platelets partially restored metastasis in both thrombocytopenic and *PF4-Cre-α6*$^{-/-}$ mice, confirming that the protective effect is platelet specific and does not rely on the absence of α6β1 integrin on any other cell type. In addition, we previously reported that platelets from *PF4-Cre-α6*$^{-/-}$ mice expressed normal levels of the main adhesion receptors (21), further pointing towards a specific role for α6β1. Blood platelets express two additional members of the β1 integrin family, namely α2β1 and α5β1. Whether one of these two platelet β1 integrins also participates in metastasis remains unknown. Although it might be tempting to speculate that neither of them is critical, since the reduction of tumor metastasis in *PF4-Cre-α6*$^{-/-}$ mice was very similar to that in *PF4-Cre-β1*$^{-/-}$ animals, future studies are warranted to investigate this issue in detail.

Our results point to a prometastatic function of ADAM9 expressed on breast and colon cancer cells in an immunocompetent mouse model. These observations are in line with a previous study in which downregulation of ADAM9 in cystic carcinoma cells led to less lung metastasis, as determined by i.v. injection into nude mice (36). In agreement, overexpression of ADAM9 in lung cancer cells resulted in both brain and lung metastases, whereas mock-transfected cells only colonized the lungs (37, 38). All these results are in accordance with clinical observations indicating that expression of ADAM9 was correlated with shortened survival and poor outcome of cancer patients and associated with the occurrence of distant metastases (39–41). ADAM9 was reported to be expressed by several malignancies, including renal, prostate, thyroid, gastric, breast, and non–small-cell lung cancer cells, highlighting its potentially broader importance in neoplasia (38, 39, 42–46). Moreover, ADAM9 overexpression was shown to be associated with poor differentiation, tumor aggressiveness, and shortened survival in patients with pancreatic tumors (47). Nevertheless, suggesting that ADAM9 might represent an attractive target for numerous cancers appears premature, since ablation of ADAM9 in tumor-associated fibroblasts has been reported to enhance tumor growth (48). Therefore, questions around the cell-specific function of ADAM9 in metastasis still need to be fully elucidated.

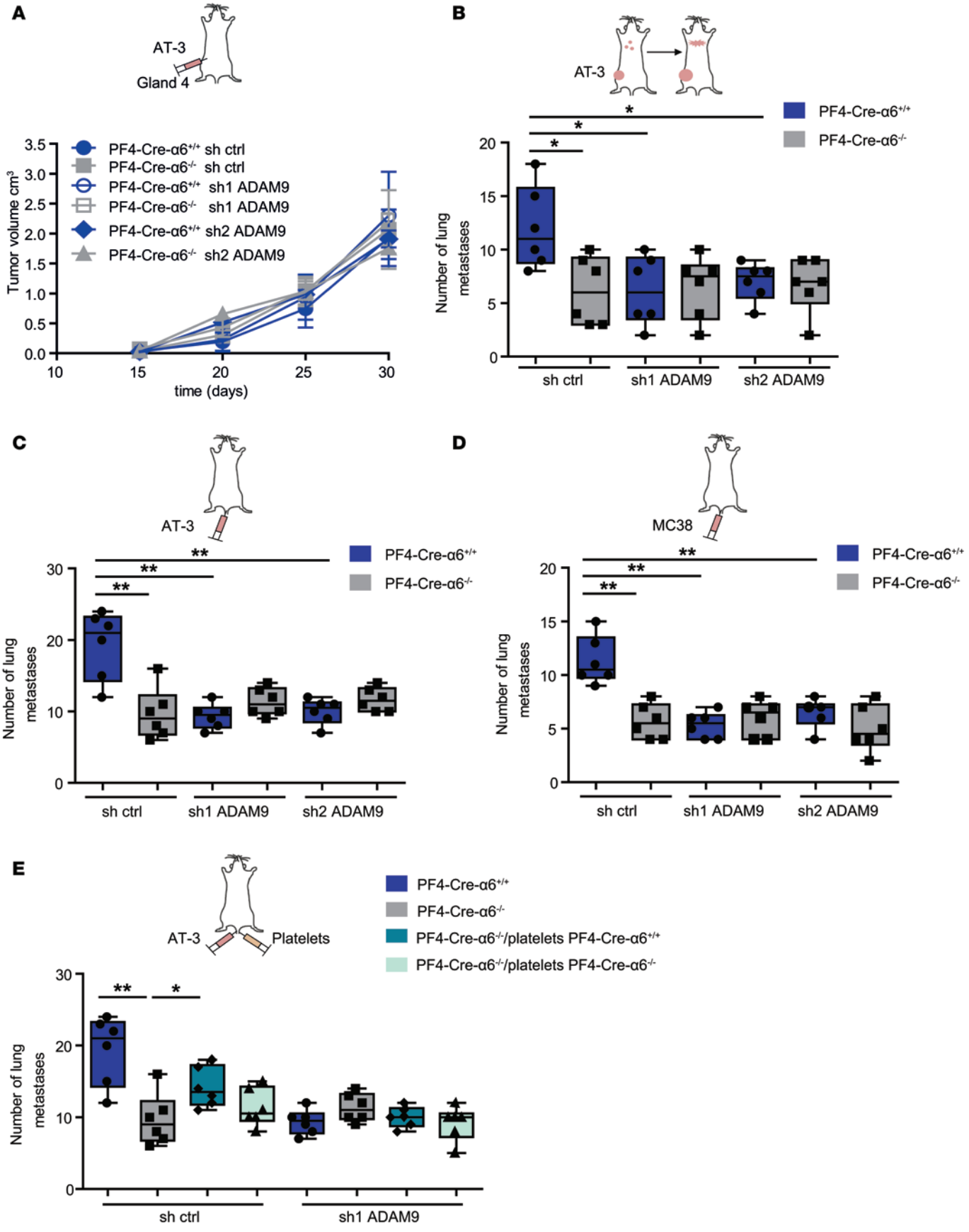
A
AT-3
Gland 4
Tumor volume cm³
time (days)
PF4-Cre-α6+/+ sh ctrl
PF4-Cre-α6-/- sh ctrl
PF4-Cre-α6+/+ sh1 ADAM9
PF4-Cre-α6-/- sh1 ADAM9
PF4-Cre-α6+/+ sh2 ADAM9
PF4-Cre-α6-/- sh2 ADAM9
B
AT-3
Number of lung metastases
PF4-Cre-α6+/+
PF4-Cre-α6-/-
sh ctrl
sh1 ADAM9
sh2 ADAM9
C
AT-3
Number of lung metastases
PF4-Cre-α6+/+
PF4-Cre-α6-/-
sh ctrl
sh1 ADAM9
sh2 ADAM9
D
MC38
Number of lung metastases
PF4-Cre-α6+/+
PF4-Cre-α6-/-
sh ctrl
sh1 ADAM9
sh2 ADAM9
E
AT-3
Platelets
PF4-Cre-α6+/+
PF4-Cre-α6-/-
PF4-Cre-α6-/-/platelets PF4-Cre-α6+/+
PF4-Cre-α6-/-/platelets PF4-Cre-α6-/-
Number of lung metastases
sh ctrl
sh1 ADAM9

Figure 4. ADAM9 on tumor cells mediates lung metastasis through platelet integrin α6β1. sh control and sh ADAM9 tumor cells (sh1 and sh2) were injected into (**A** and **B**) the mammary fat pad region (AT-3 cells) or (**C**–**E**) directly in tail veins (AT-3 or MC38) of *PF4-Cre-α6*$^{+/+}$ and *PF4-Cre-α6*$^{-/-}$ mice. (**E**) *PF4-Cre-α6*$^{+/+}$ and *PF4-Cre-α6*$^{-/-}$ mice were transfused with *PF4-Cre-α6*$^{+/+}$ and *PF4-Cre-α6*$^{-/-}$ platelets and injected collaterally with AT-3 cells (sh ctrl or sh1 ADAM9). (**A**) Volumes of primary tumors (AT-3) were determined at the indicated days after tumor cell injection. Six mice per each group were used. (**B**) Spontaneous and (**C**–**E**) experimental lung metastasis were determined at 30 (AT-3) or 20 (AT-3 or MC38) days of after injection, respectively. Quantification of (**A**) mammary tumor volume and (**B**–**E**) metastatic foci in lung sections of *PF4-Cre-α6*$^{+/+}$ and *PF4-Cre-α6*$^{-/-}$ mice. $*P < 0.05$, $**P < 0.01$, Mann-Whitney test. Each point represents an individual mouse. (**B**–**E**) Box-and-whisker plots were used to graphically represent the median (line within box), upper and lower quartile (bounds of box), and maximum and minimum values (bars).

Our results identified α6β1 as a receptor supporting efficient adhesion of platelets to tumor cells through direct interaction with ADAM9. We also demonstrated that this molecular interaction led to platelet activation, as evidenced by a defective platelet shape change on DC-9 when α6β1 is absent. This result demonstrates that ADAM9 is able to initiate an intraplatelet signal downstream of α6β1. Whether this signaling is similar to that initiated by the typical α6β1 ligands, laminins, requires further detailed investigation. ADAM9-induced signals result not only in a platelet shape change, but also in P-selectin exposure, indicating that granule secretion occurs. Platelet granules contain many bioactive molecules, including TGF-β and ADP and ATP, which were previously described to modulate directly or indirectly the metastatic potential of tumor cells (9, 13, 49). Platelet release of TGF-β is a well-accepted event by which platelets enhance the invasiveness of tumor cells notably by promoting epithelial-to-mesenchymal transition (9). Besides, ATP secreted from activated platelets was reported to bind the endothelial $P2Y_2$ receptor, promoting vascular permeability and thereby facilitating tumor cell extravasation (13). Altogether, we propose a working model, whereby platelet α6β1 binding to ADAM9 on tumor cells promotes platelet activation and the subsequent secretion of the granule contents. The bioactive molecules released by activated platelets could in turn promote tumor cell extravasation either indirectly by inducing vascular permeability or directly by promoting tumor cell invasiveness, ultimately leading to metastasis of distant organs (Figure 7).

We provided evidence that i.v. injection of GoH3, an integrin α6-blocking antibody that prevents platelet-tumor cell crosstalk, diminished lung metastasis in WT mice. This observation opens up the intriguing possibility of developing a therapeutic strategy aimed at targeting this integrin to interfere with tumor cell dissemination in cancer patients. Of note, this blocking antibody did not provoke a thrombocytopenia, suggesting that such a pharmacological approach would preserve a normal platelet count. In addition, since platelet integrin α6β1 appears dispensable for normal hemostasis (21), one could hypothesize that targeting this integrin would also avoid bleeding complications. This is of importance since currently used antiplatelet drugs are known to increase the bleeding risk that complicates their use in clinical settings (50–53). Besides, the specificity of pharmacologically targeting platelet α6β1 was evidenced by the loss of protective effect when GoH3 was administrated to *PF4-Cre-α6*$^{-/-}$ mice. This observation suggests that such an approach would primarily act through α6β1 expressed on platelets to prevent metastasis. Preclinical studies are necessary to identify the stage at which such a therapeutic approach would confer an optimal antimetastatic effect as well as potential side effects due to long-term treatment. It has been reported that defects in α6 integrin result in hemidesmosome deficiency and cause skin and mucous membrane disorders, such as pyloric atresia and epidermolysis bullosa, and, in most cases, early postnatal death (54, 55). Whether a pharmacological strategy would result in such pathologies occurring during development is uncertain but will need to be tested. Future studies might also highlight a potential net benefit of targeting other cellular pools of this integrin, since some of them, notably those expressed on endothelial or tumor cells, also actively participate in cancer progression (22–27).

In conclusion, our study reveals a major contribution of integrin α6β1 to platelet interaction with tumor cells through the binding of ADAM9. This interaction promotes platelet activation, granule secretion, and subsequent endothelial transmigration of tumor cells, ultimately promoting tumor metastasis. Finally, we propose that targeting α6β1 may offer a potentially interesting antimetastatic strategy to be used in conjunction with traditional strategies.

Methods

Animals. C57BL/6 mice were obtained from Charles River Laboratories. *PF4-Cre* and *c-mpl*$^{-/-}$ mice were provided by Radek Skoda (Experimental Hematology, University Hospital Basel, Basel, Switzerland). *PF4-Cre-α6*$^{-/-}$ and their littermate control *PF4-Cre-α6*$^{+/+}$ mice were generated as previously described (21). To generate mice lacking integrin β1 in platelets, C57BL/6 mice containing the *Itgβ1* gene flanked by loxP

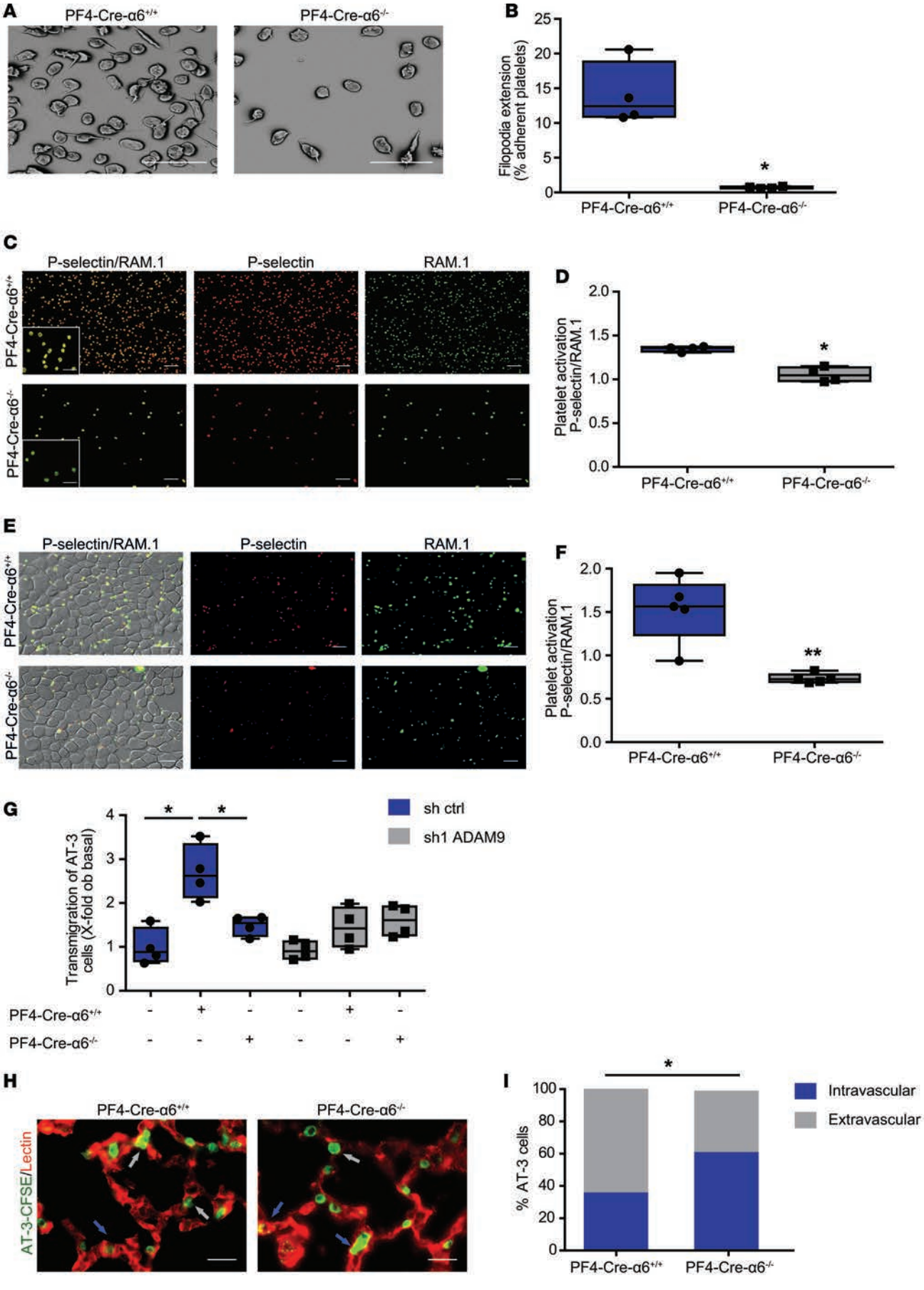
A
PF4-Cre-α6+/+
PF4-Cre-α6-/-
B
Filopodia extension (% adherent platelets)
25
20
15
10
5
0
*
PF4-Cre-α6+/+
PF4-Cre-α6-/-
C
P-selectin/RAM.1
P-selectin
RAM.1
PF4-Cre-α6+/+
PF4-Cre-α6-/-
D
Platelet activation P-selectin/RAM.1
2.0
1.5
1.0
0.5
0.0
*
PF4-Cre-α6+/+
PF4-Cre-α6-/-
E
P-selectin/RAM.1
P-selectin
RAM.1
PF4-Cre-α6+/+
PF4-Cre-α6-/-
F
Platelet activation P-selectin/RAM.1
2.0
1.5
1.0
0.5
0.0
**
PF4-Cre-α6+/+
PF4-Cre-α6-/-
G
sh ctrl
sh1 ADAM9
Transmigration of AT-3 cells (X-fold ob basal)
4
3
2
1
0
*
*
PF4-Cre-α6+/+ - + - - + -
PF4-Cre-α6-/- - - + - - +
H
PF4-Cre-α6+/+
PF4-Cre-α6-/-
AT-3-CFSE/Lectin
I
% AT-3 cells
100
80
60
40
20
0
*
Intravascular
Extravascular
PF4-Cre-α6+/+
PF4-Cre-α6-/-

Figure 5. Platelet integrin α6β1 promotes platelet activation and granule release and enhances tumor cell extravasation through ADAM9. Representative (**A**) scanning electron microscopy and (**C**) immunofluorescence microscopy images of *PF4-Cre-α6*$^{+/+}$ and *PF4-Cre-α6*$^{-/-}$ mouse platelets adhering to recombinant DC-9 under (**A** and **B**) flow and (**C** and **D**) static conditions, respectively. (**A** and **B**) Hirudinated mouse whole blood was perfused over DC-9 (500 μg/ml) at 300 s^{-1}. (**A**) The morphology of adherent platelets was examined after 3 minutes by scanning electron microscopy, and (**B**) the percentage of platelets extending filopodia was quantified. Scale bar: 8 μm. Mean ± SEM. *P < 0.05, Mann-Whitney test. (**C**–**F**) Washed *PF4-Cre-α6*$^{+/+}$ and *PF4-Cre-α6*$^{-/-}$ mouse platelets were allowed to adhere to (**C**) DC-9 (500 μg/ml) or (**E**) AT-3 cells. After 30 minutes, adherent platelets were stained with the anti-GPIbβ antibody, RAM.1 (green), and for P-selectin exposure (red). (**C** and **E**) Representative immunofluorescence staining of platelets adhered on (**C**) DC-9 or (**E**) AT-3 cells. Scale bar: 20 μm; 10 μm (inset). (**D** and **F**) Quantification of the ratio between P-selectin and RAM.1 signals of adherent platelets. *P < 0.05, **P < 0.01, Mann-Whitney test. Each point represents an individual mouse. (**G**) AT-3 control or ADAM9-silenced cancer cells were seeded on HUVECs, and tumor cell transmigration was determined in the absence or presence of PF4-Cre-α6$^{+/+}$ and PF4-Cre-α6$^{-/-}$ platelets. *P < 0.05, Mann-Whitney test. Each point represents a separate experiment. (**H**) Representative fluorescent microscopy images of lung sections of *PF4-Cre-α6*$^{+/+}$ and *PF4-Cre-α6*$^{-/-}$ mice 6 hours after i.v. injection of AT-3-CFSE cells (green). Lung vessels were stained with lectin (red). Gray and blue arrows indicate extravascular and intravascular cells, respectively. Scale bar: 10 μm. (**I**) The percentage of intravascular and extravascular AT-3 cells in lungs of *PF4-Cre-α6*$^{+/+}$ and *PF4-Cre-α6*$^{-/-}$ mice. *P < 0.05, Fisher's exact test. Four mice per each group were used. (**B**, **D**, **F**, and **G**) Box-and-whisker plots were used to graphically represent the median (line within box), upper and lower quartile (bounds of box), and maximum and minimum values (bars).

sites, β1$^{fl/fl}$, were crossed with *PF4-Cre* mice (provided by Reinhard Fässler, Max Planck Institute of Biochemistry, Martinsried, Germany). All experiments with animals were performed in accordance with French legislation and INSERM guidelines and followed the recommendations of the *Guide for the Care and Use of Laboratory Animals* (National Academies Press. 2011).

Cell culture. Cell lines were cultured in a humidified incubator with 5% CO_2 at 37°C. The PyMT cells, termed AT-3 cells, were isolated from a mammary carcinoma of MMTV-PyMT transgenic mice in a C57BL/6 background, as previously described (56). AT-3, B16-F10 (mouse melanoma, ATCC CRL-6475), MDA-MB-231 (human breast carcinoma, ATCC HTB-26), SKRB3 (human breast carcinoma, ATCC HTB-30), and LoVo (colon carcinoma, ATCC CCL-229) cells were maintained in DMEM (CliniSciences). E0771 mouse medullary mammary adenocarcinoma (tebu-bio) and MC38 mouse colon carcinoma (provided by Pedro Berraondo Lopez, University of Navarra, Pamplona, Spain) cell lines were cultured in RPMI 1640 medium (CliniSciences). All media were supplemented with fetal bovine serum (Biowest) 10%, penicillin-streptomycin 1% (Gibco). HUVECs were grown according to the manufacturer's instructions (Promocell).

Establishment of ADAM9 knockdown cells. Human embryonic kidney 293T (HEK293T) cells were transfected with pGFP-C sh human ADAM9 (sh1: TL314947A CTTGCTGCGAAGGAAGTACCTGTAAGCTT) lentiviral vector, pGFP-C sh mouse ADAM9 (sh1: TL500040B CAACGTACAGAGCCATTGTCACTATCGAG, sh2: TL500040D: GGTATGTAACAGCAATAAGAATTGTCACT) lentiviral vector, or pGFP-C short hairpin RNA control (sh ctrl) lentiviral vector (TR30021) containing a noneffective 29-mer scrambled shRNA cassette (OriGene, CliniSciences) together with pLP1, pLP2, and pLP/VSVG vectors (Life Technologies) to obtain lentiviral particles. After 48 hours, conditioned media from HEK293T cells were collected, centrifuged to remove cell debris, and used to transduce AT-3, MC-38, and MDA-MB-231 cells in the presence of 5 μg/ml polybrene (Sigma-Aldrich), followed by selection with puromycin (1.5–2 μg/ml) (Sigma-Aldrich). Expression of ADAM9 was determined by quantitative real-time PCR (qRT-PCR) and immunofluorescence staining.

qRT-PCR. Total RNA from cell lines or mouse lungs was extracted with TriReagent according to the manufacturer's instructions (Life Technologies). RNA was treated with DNaseI and reverse transcribed using the High-Capacity cDNA RT Kit (Life Technologies). qRT-PCR was performed using the Power SYBR Green PCR Master Mix (Life Technologies) according to the manufacturer's protocol. Relative values of gene expression were normalized to GAPDH, and fold change in relative expression was determined by calculating $2^{-\Delta\Delta Ct}$, where ΔΔCt = (ΔCt target gene – ΔCt GAPDH) sample – (ΔCt target gene – ΔCt GAPDH) control. Primer sequences are listed in Supplemental Table 1.

Expression and purification of DC-9. Recombinant DC-9 was produced as previously described (33). Briefly, HEK293-EBNA cells were transfected by JetPei (Polyplus) with pCEP-pu BM40-cHis-Dis-Cys plasmid giving rise to a fusion protein with a His6 tag placed in frame with disintegrin-cysteine-rich coding regions of ADAM9. Then, supernatants were collected and proteins were purified by metal affinity chromatographic columns (CliniSciences).

Experimental and spontaneous models of metastasis. For experimental metastasis models, 3×10^5 B16F10, E0771, AT-3, and MC38 parental cells or sh ctrl or sh ADAM9 clones in 200 μl of cell media were injected into a lateral tail vein of each mouse. Mice were sacrificed on day 20 after tumor cell inoculation, and the

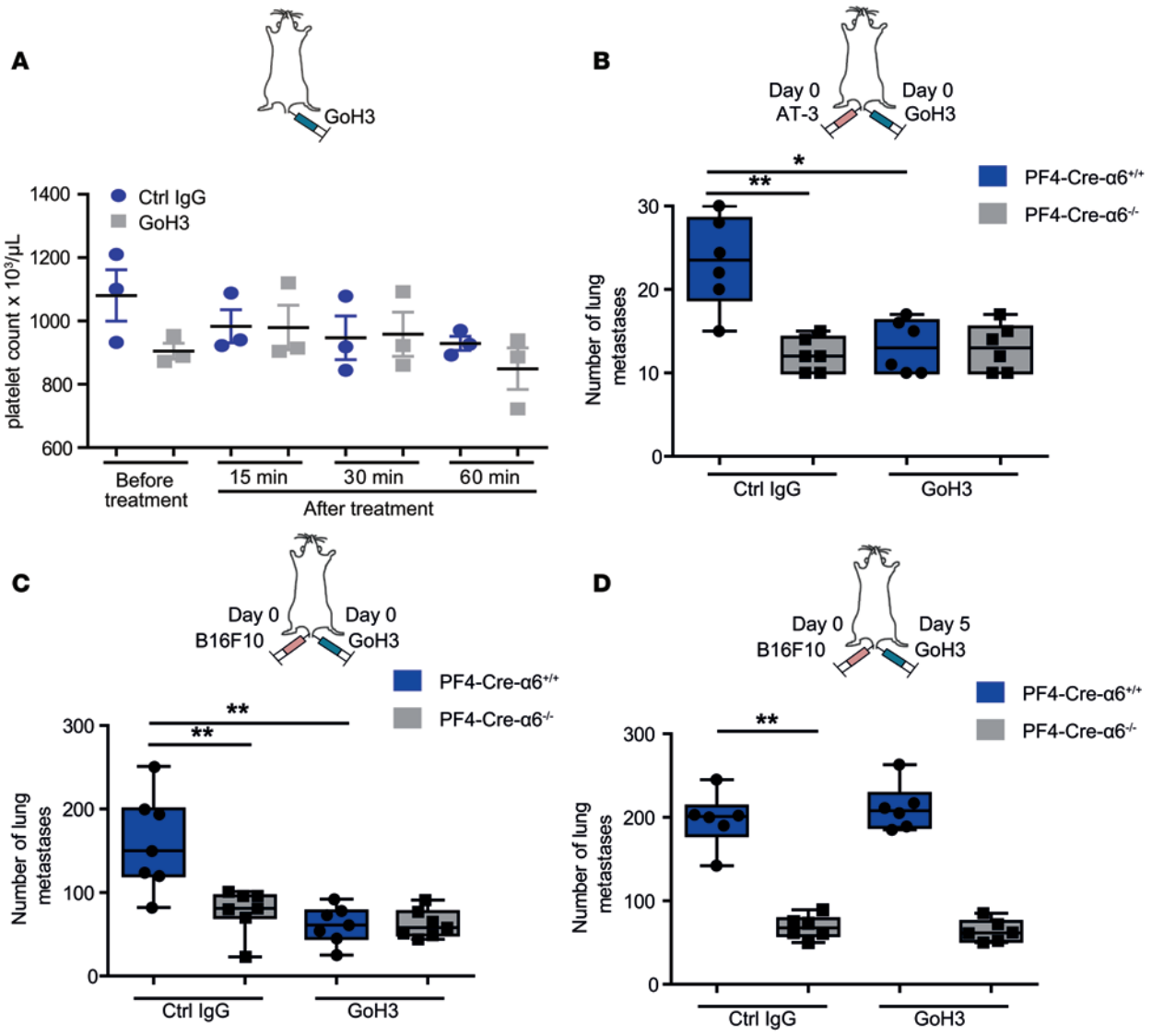

Figure 6. Antibody-mediated blockade of α6β1 integrin inhibits tumor metastasis. (**A**) Effect of the injection of GoH3, an α6-blocking antibody, on platelet count. C57BL/6 mice were injected with 2 mg/kg GoH3 or irrelevant control IgG, and 15, 30, and 60 minutes later the platelet count was determined. Horizontal black bars denote the mean. Mean ± SEM. (**B**–**D**) *PF4-Cre-α6*$^{+/+}$ and *PF4-Cre-α6*$^{-/-}$ mice were i.v. injected with GoH3 or a control antibody in parallel with indicated tumor cells at indicated times. Numbers of metastatic foci in lung tissues of (**B**) AT-3–injected or (**C** and **D**) B16F10-injected *PF4-Cre-α6*$^{+/+}$ and *PF4-Cre-α6*$^{-/-}$ mice. *$P < 0.05$, **$P < 0.01$, Mann-Whitney test. Each point represents an individual mouse. (**B**–**D**) Box-and-whisker plots were used to graphically represent the median (line within box), upper and lower quartile (bounds of box), and maximum and minimum values (bars).

number of metastases was determined by counting metastatic foci on the lung surface (B16F10 model) and histopathological analysis (as described below). For orthotopic breast cancer models, 2×10^5 parental AT-3 or AT-3 sh ctrl and AT-3 sh ADAM9 cells were injected into the mammary fat pads of 8-week-old female virgin mice, which were sacrificed on day 30. Primary tumor volumes were measured using Vernier calipers and determined using following calculation: volume = $(\text{width})^2 \times \text{length}/2$.

H&E staining. Lung tissues were collected and fixed in 4% PFA and then dehydrated in sucrose 20% and embedded in OCT medium and cross sectioned (7 µm). Tissue sections were stained with hematoxylin for 5 minutes and washed with running tap water. Differentiation was accomplished in acid alcohol for 10 seconds followed by washing for 10 minutes. Tissues sections were incubated in eosin for 20 seconds, rinsed, and mounted using the Savemount reagent (vwr chemicals, BDH Prolabo). Stained tissues were observed under a light microscope (Zeiss Imager Z2 inverted microscope and AxioVision software, Carl Zeiss), and metastases were counted by two separate experimenters.

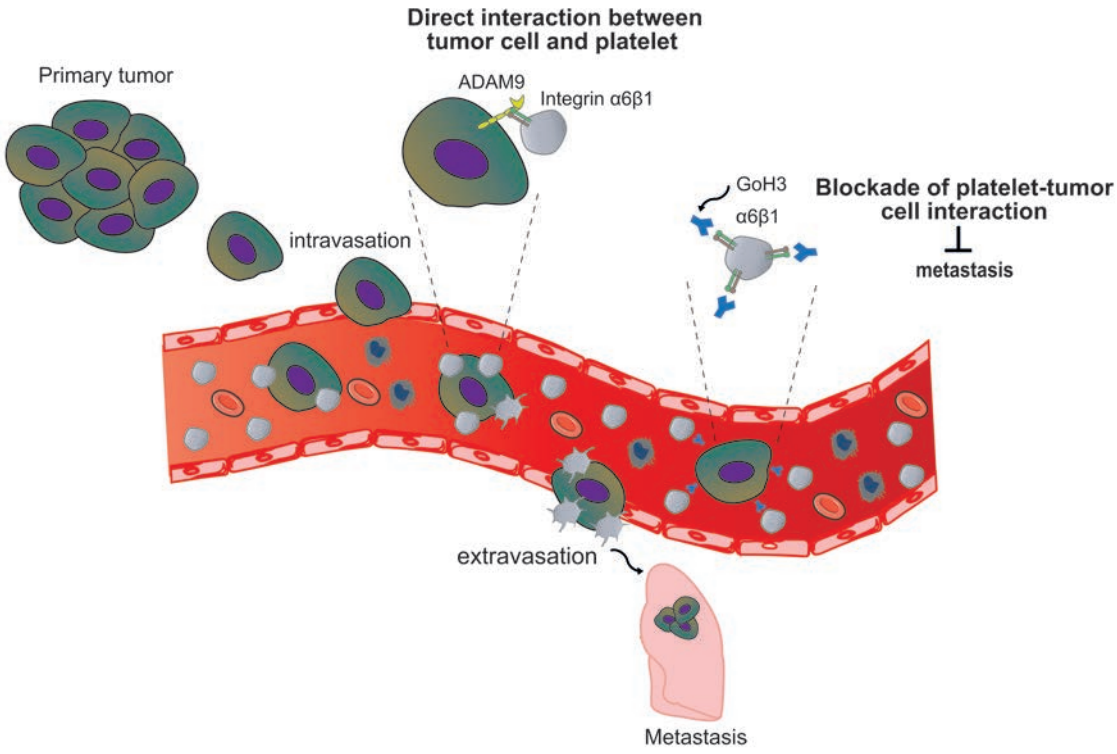

Figure 7. Schematic overview of the role of platelet integrin α6β1 in tumor metastasis. Following entry of tumor cells into the bloodstream, platelet integrin α6β1 favors platelet recruitment to circulating tumor cells through its direct binding to ADAM9 on tumor cells. Once stable interaction is established, platelets become activated and could protect tumor cells from shear stress and host immune system and favor efficient tumor cell extravasation and subsequent metastasis. A function-blocking anti-integrin α6 antibody, GoH3, attenuated the occurrence of metastases by preventing platelet-tumor cell crosstalk.

Blood counts. C57BL/6 mice were injected with α6-blocking antibody (2 mg/kg, GoH3, Santa Cruz Biotechnology) or irrelevant control IgG (2 mg/kg, BD Biosciences). Blood samples were collected from individual mice, and the mouse blood cell count was analyzed using ABC Vet analyzer (SCIL).

Preparation of washed platelets. Blood was drawn from the abdominal aorta of adult mice anesthetized intraperitoneally with a mixture of xylazine (20 mg/kg, Rompun, Bayer) and ketamine (100 mg/kg, Imalgene 1,000, Merial). Human blood was collected from healthy volunteers who had not taken any antiplatelet medication in the preceding 2 weeks. Platelets were washed using ACD-anticoagulated whole blood as previously described (57).

Platelet transfusion. 1 $\times 10^9$ washed mouse (PF4-Cre-α6+/+ or PF4-Cre-α6–/–) platelets in Tyrode's buffer were injected i.v. into indicated mice via a lateral tail vein.

In vitro platelet adhesion assay. Murine (parental, sh ctrl or sh ADAM9 AT-3, and MC38) or human (parental MDA-MB-231, sh ctrl MDA-MB-231, sh ADAM9 MDA-MB-231, and SKRB3, LoVo) tumor cell lines were seeded into LabTek chamber slides (Labtek) at a concentration of 3×10^5 per well. Washed murine (PF4-Cre-α6+/+ or PF4-Cre-α6–/–) or human platelets incubated with antibodies directed against integrin α6 (GoH3, Santa Cruz Biotechnology) and integrin β1 (P5D2, Santa Cruz Biotechnology) were allowed to adhere to murine or human tumor cells for 15 minutes. To assess activation of platelets the time of experiment was prolonged up to 30 minutes at 37°C. After washing with PBS 1×, chambers were fixed in PFA 4% for 20 minutes and then washed with PBS 1× and incubated overnight with an antibody against P-selectin (1 μg/ml, CLB-Thromb/6, Beckman Coulter). The next day, chambers were incubated for 1 hour with Cy-3–conjugated goat anti-rabbit IgG (1 μg/ml, Jackson ImmunoResearch Laboratories) and stained with Alexa 488–coupled RAM.1 antibody (5 μg/ml) (58). Chambers were mounted and 5 pictures were taken for each condition. Quantification of immunofluorescence signals was obtained using ImageJ software (NIH) and the analyze particle module.

Immunofluorescence staining. AT-3 sh ctrl or sh ADAM9 cells were labeled for 15 minutes at 37°C with 10 μg/ml CFSE (Life Technologies) in serum-free medium and washed twice with PBS 1×, and 1×10^6 cells

were i.v. injected into the tail veins of *c-mpl*$^{-/-}$, *PF4-Cre-α6*$^{+/+}$, or *PF4-Cre-α6*$^{-/-}$ mice. In some experiments, the mice were i.v. injected with DyLight 594–Lycopersicon esculentum (Tomato) lectin (100 μl per mouse) 30 minutes, 2 hours, 4 hours, and 6 hours later. After 10 minutes, lungs were collected as described above and cryosectioned (10 μm) for fluorescence imaging to visualize the vasculature (red) and tumor cells (green). For platelet immunostaining in lungs, 7-μm-thick sections were incubated for 1 hour with Cy-3–conjugated RAM.1 antibody (5 μg/ml). For immunostaining in cell cultures, B16F10, E0771, MDA-MB-231, SKRB3, LoVo, AT-3 sh ctrl or sh ADAM9 cells, and MC38 sh ctrl or sh ADAM9 tumor cells were fixed with PFA 4% in PBS 1× for 15 minutes, washed and blocked in PBS 1× 5% normal goat serum, followed by a staining with the primary antibody against ADAM9 (0.5 μg/ml AB2959, Chemicon, Millipore). After washing, cells were incubated for 1 hour with Cy-3–conjugated goat anti-rabbit IgG (1 μg/ml, Jackson ImmunoResearch Laboratories). Tissue sections and cell cultures were counterstained with DAPI (1:36:000), mounted using the FluorSave reagent (Calbiochem), and observed with an epifluorescence microscope (Leica Microsystems) and ×63 oil immersion objective. Tumor cells overlapping with vasculature were scored as intravascular, while cells outside blood vessels were scored as extravascular.

Static adhesion assay. Glass coverslips were coated with recombinant DC-9 (500 μg/ml) for 2 hours at room temperature and blocked with human serum albumin (HSA) 1% in PBS 1× for 60 minutes. *PF4-Cre-α6*$^{+/+}$ and *PF4-Cre-α6*$^{-/-}$ mouse platelets (4.5×10^6/coverslip) in Tyrode's buffer were allowed to adhere to the coated surfaces at 37°C. After 1 hour, nonadherent platelets were washed away and adherent cells were fixed with PFA 4% in PBS 1× and then stained with Alexa 488–conjugated RAM.1 (5 μg/ml) and P-selectin antibody (1 μg/ml, CLB-Thromb/6, Beckman Coulter). Coverslips were mounted and then observed with epifluorescence microcopy (Leica Microsystems) and ×40× and ×100 oil immersion objectives. Ten pictures were taken per each condition, and platelet adhesion was calculated using ImageJ software.

Flow-mediated platelet adhesion. Adhesion assays in a flow system were performed as previously described (59). Microcapillaries were coated with recombinant DC-9 (500 μg/ml) and passivated with 1% HSA 1% in PBS 1× for 30 minutes at room temperature. Hirudinated (100 U/ml, Transgene) *PF4-Cre-α6*$^{+/+}$ and *PF4-Cre-α6*$^{-/-}$ mouse whole blood was perfused through the microcapillaries for 3 minutes, at 300 s^{-1}, using a programmable syringe pump (PHD 2000, Harvard Apparatus). Platelet adhesion was observed with a Leica DMI 4000 B (Leica Microsystems) using a ×63, 1.4 numerical aperture oil objective and differential interference contrast microscopy, equipped with a CCD CoolSNAP HQ Monochrome camera (Photometrics). Platelet adhesion was analyzed using Metamorph software version 7.6 (Molecular Devices).

Scanning electron microscopic analysis of the morphological changes of platelets after adhesion to DC-9. Hirudinated (100 U/ml) mouse whole blood was perfused through glass microcapillaries coated with recombinant DC-9 (500 μg/ml) for 3 minutes, at 300 s^{-1}, followed by washing with PBS 1× at 300 s^{-1}. Scanning electron microscopy was performed as described elsewhere (60). Change in cell shape was defined as the transformation of a resting discoid platelet into an activated spherical cell with filopodial projections of more than 0.2 μm in length.

Transwell assay. HUVECs (50,000 at seeding in 50 μl) were cultured for 2 days on 96-well Transwell plates with a 8-μm pore size polyester membrane (Sigma-Aldrich) with medium changes every day. Media from the upper compartment were removed and 50 μl of CFSE-labeled AT-3 sh ctrl or AT-3 sh ADAM9 tumor cells (8×10^5/ml) in Tyrode's buffer alone or together with a 1:1 mixture of platelets (2×10^8/ml) was added to the upper compartment. In all experiments, 250 μl Tyrode's buffer or culture media was added to the lower compartment and tumor cells were allowed to transmigrate overnight. On the next day, the nontransmigrated tumor cells from the upper compartment were removed, and only the transmigrated tumor cells on the lower side of the filter or the bottom of the Transwell insert were imaged with an epifluorescence microscope (Leica Microsystems) and quantified with ImageJ. Each experiment was performed 4 times with 5 wells per condition.

Statistics. The statistical significance of results was analyzed using the GraphPad Prism program, version 5.0. The Shapiro-Wilk normality test was used to confirm the normality of the data, and the statistical difference of the mean was analyzed using the Student's unpaired 2-tailed *t* test. For data not following a Gaussian distribution, the nonparametric Mann-Whitney test was used. Contingency was analyzed using the Fisher's exact test. *P* values of less than 0.05 were considered to be significant.

Study approval. Murine experiments were performed according to French regulations and were approved by the Regional Ethical Committee for Animal Experimentation of Strasbourg (C.R.E.M.E.A.S., CEEA 35) (approval no. for animal experiments: 2015082714213372).

Author contributions

EMB conceived and designed the research, acquired and analyzed the data, and wrote the manuscript. C Brucker, C Bourdon, and MF acquired and analyzed the data. PZ, ADA, SIA, and GO provided essential tools and contributed to the writing of manuscript. CG interpreted the data, contributed to the writing of manuscript, and acquired the funding. PHM conceived and designed the research, interpreted the data, cowrote the manuscript, and acquired the funding.

Acknowledgments

The authors would like to thank Catherine Ziessel, Jean-Yves Rinckel, Sebastien Egard, and Nicolas Receveur (UMR-S949, INSERM, Etablissement Français du Sang-Alsace) for technical assistance and Pedro Berraondo Lopez for MC38 cells (University of Navarra, Spain). This work was supported by INSERM, Etablissement Français du Sang, Association de Recherche et Développement en Médecine et Santé Publique, and Institut National du Cancer (grant no. PLBIO13-079).

Address correspondence to: Pierre Henri Mangin, UMR-S949, INSERM, Université de Strasbourg, Etablissement Français du Sang-Alsace (EFS-Alsace), 10 rue Spielmann, BP no. 36, 67065 Strasbourg Cedex, France. Phone: 33.38.21.25.25; E-mail: pierre.mangin@efs.sante.fr.

1. Quail DF, Joyce JA. Microenvironmental regulation of tumor progression and metastasis. *Nat Med*. 2013;19(11):1423–1437.
2. Reymond N, d'Água BB, Ridley AJ. Crossing the endothelial barrier during metastasis. *Nat Rev Cancer*. 2013;13(12):858–870.
3. Nguyen DX, Bos PD, Massagué J. Metastasis: from dissemination to organ-specific colonization. *Nat Rev Cancer*. 2009;9(4):274–284.
4. Luzzi KJ, et al. Multistep nature of metastatic inefficiency: dormancy of solitary cells after successful extravasation and limited survival of early micrometastases. *Am J Pathol*. 1998;153(3):865–873.
5. Labelle M, Hynes RO. The initial hours of metastasis: the importance of cooperative host-tumor cell interactions during hematogenous dissemination. *Cancer Discov*. 2012;2(12):1091–1099.
6. Mammadova-Bach E, Mangin P, Lanza F, Gachet C. Platelets in cancer. From basic research to therapeutic implications. *Hamostaseologie*. 2015;35(4):325–336.
7. Nieswandt B, Hafner M, Echtenacher B, Männel DN. Lysis of tumor cells by natural killer cells in mice is impeded by platelets. *Cancer Res*. 1999;59(6):1295–1300.
8. Palumbo JS, et al. Platelets and fibrin(ogen) increase metastatic potential by impeding natural killer cell-mediated elimination of tumor cells. *Blood*. 2005;105(1):178–185.
9. Labelle M, Begum S, Hynes RO. Direct signaling between platelets and cancer cells induces an epithelial-mesenchymal-like transition and promotes metastasis. *Cancer Cell*. 2011;20(5):576–590.
10. Läubli H, Borsig L. Selectins promote tumor metastasis. *Semin Cancer Biol*. 2010;20(3):169–177.
11. Kim YJ, Borsig L, Han HL, Varki NM, Varki A. Distinct selectin ligands on colon carcinoma mucins can mediate pathological interactions among platelets, leukocytes, and endothelium. *Am J Pathol*. *1999*;155(2):461–472.
12. Konstantopoulos K, Thomas SN. Cancer cells in transit: the vascular interactions of tumor cells. *Annu Rev Biomed Eng*. 2009;11:177–202.
13. Schumacher D, Strilic B, Sivaraj KK, Wettschureck N, Offermanns S. Platelet-derived nucleotides promote tumor-cell transendothelial migration and metastasis via P2Y2 receptor. *Cancer Cell*. 2013;24(1):130–137.
14. Gay LJ, Felding-Habermann B. Contribution of platelets to tumour metastasis. *Nat Rev Cancer*. 2011;11(2):123–134.
15. Cox D, Brennan M, Moran N. Integrins as therapeutic targets: lessons and opportunities. *Nat Rev Drug Discov*. 2010;9(10):804–820.
16. Desgrosellier JS, Cheresh DA. Integrins in cancer: biological implications and therapeutic opportunities. *Nat Rev Cancer*. 2010;10(1):9–22.
17. Takagi S, et al. Platelets promote tumor growth and metastasis via direct interaction between Aggrus/podoplanin and CLEC-2. *PLoS One*. 2013;8(8):e73609.
18. Bakewell SJ, et al. Platelet and osteoclast beta3 integrins are critical for bone metastasis. *Proc Natl Acad Sci U S A*. 2003;100(24):14205–14210.
19. Zhang C, et al. Modified heparins inhibit integrin alpha(IIb)beta(3) mediated adhesion of melanoma cells to platelets in vitro and in vivo. *Int J Cancer*. 2009;125(9):2058–2065.
20. Zhang W, et al. A humanized single-chain antibody against beta 3 integrin inhibits pulmonary metastasis by preferentially fragmenting activated platelets in the tumor microenvironment. *Blood*. 2012*;120(*14):2889–2898.
21. Schaff M, et al. Integrin α6β1 is the main receptor for vascular laminins and plays a role in platelet adhesion, activation, and arterial thrombosis. *Circulation*. 2013;128(5):541–552.
22. Lu X, Lu D, Scully M, Kakkar V. The role of integrins in cancer and the development of anti-integrin therapeutic agents for cancer therapy. *Perspect Medicin Chem*. 2008;2:57–73.
23. Lamb LE, Zarif JC, Miranti CK. The androgen receptor induces integrin α6β1 to promote prostate tumor cell survival via NF-κB and Bcl-xL Independently of PI3K signaling. *Cancer Res*. 2011;71(7):2739–2749.
24. Seano G, et al. Endothelial podosome rosettes regulate vascular branching in tumour angiogenesis. *Nat Cell Biol*. 2014;16(10):931–941.
25. Ports MO, Nagle RB, Pond GD, Cress AE. Extracellular engagement of alpha6 integrin inhibited urokinase-type plasminogen activator-mediated cleavage and delayed human prostate bone metastasis. *Cancer Res*. 2009;69(12):5007–5014.

26. Primo L, et al. Increased expression of alpha6 integrin in endothelial cells unveils a proangiogenic role for basement membrane. *Cancer Res*. 2010;70(14):5759–5769.
27. Bouvard C, et al. Tie2-dependent deletion of α6 integrin subunit in mice reduces tumor growth and angiogenesis. *Int J Oncol*. 2014;45(5):2058–2064.
28. Nath D, Slocombe PM, Webster A, Stephens PE, Docherty AJ, Murphy G. Meltrin gamma(ADAM-9) mediates cellular adhesion through alpha(6)beta(1)integrin, leading to a marked induction of fibroblast cell motility. *J Cell Sci*. 2000;113(Pt 12):2319–2328.
29. Almeida EA, et al. Mouse egg integrin alpha 6 beta 1 functions as a sperm receptor. *Cell*. 1995;81(7):1095–1104.
30. Murphy G. The ADAMs: signalling scissors in the tumour microenvironment. *Nat Rev Cancer*. 2008;8(12):929–941.
31. Zhou M, Graham R, Russell G, Croucher PI. MDC-9 (ADAM-9/Meltrin gamma) functions as an adhesion molecule by binding the alpha(v)beta(5) integrin. *Biochem Biophys Res Commun*. 2001;280(2):574–580.
32. Zigrino P, Nischt R, Mauch C. The disintegrin-like and cysteine-rich domains of ADAM-9 mediate interactions between melanoma cells and fibroblasts. *J Biol Chem*. 2011;286(8):6801–6807.
33. Zigrino P, et al. Role of ADAM-9 disintegrin-cysteine-rich domains in human keratinocyte migration. *J Biol Chem*. 2007;282(42):30785–30793.
34. Karadag A, Zhou M, Croucher PI. ADAM-9 (MDC-9/meltrin-gamma), a member of the a disintegrin and metalloproteinase family, regulates myeloma-cell-induced interleukin-6 production in osteoblasts by direct interaction with the alpha(v)beta5 integrin. *Blood*. 2006;107(8):3271–3278.
35. Gurney AL, Carver-Moore K, de Sauvage FJ, Moore MW. Thrombocytopenia in c-mpl-deficient mice. *Science*. 1994;265(5177):1445–1447.
36. Xu Q, Liu X, Cai Y, Yu Y, Chen W. RNAi-mediated ADAM9 gene silencing inhibits metastasis of adenoid cystic carcinoma cells. *Tumour Biol*. 2010;31(3):217–224.
37. Lin CY, et al. ADAM9 promotes lung cancer metastases to brain by a plasminogen activator-based pathway. *Cancer Res*. 2014;74(18):5229–5243.
38. Shintani Y, et al. Overexpression of ADAM9 in non-small cell lung cancer correlates with brain metastasis. *Cancer Res*. 2004;64(12):4190–4196.
39. Fritzsche FR, et al. ADAM9 expression is a significant and independent prognostic marker of PSA relapse in prostate cancer. *Eur Urol*. 2008;54(5):1097–1106.
40. Tao K, et al. Increased expression of a disintegrin and metalloprotease-9 in hepatocellular carcinoma: implications for tumor progression and prognosis. *Jpn J Clin Oncol*. 2010;40(7):645–651.
41. Yamada D, et al. Increased expression of ADAM 9 and ADAM 15 mRNA in pancreatic cancer. *Anticancer Res*. 2007;27(2):793–799.
42. Xiong Y, Kotian S, Zeiger MA, Zhang L, Kebebew E. miR-126-3p Inhibits Thyroid Cancer Cell Growth and Metastasis, and Is Associated with Aggressive Thyroid Cancer. *PLoS One*. 2015;10(8):e0130496.
43. Fritzsche FR, et al. ADAM9 is highly expressed in renal cell cancer and is associated with tumour progression. *BMC Cancer*. 2008;8:179.
44. Sung SY, et al. Oxidative stress induces ADAM9 protein expression in human prostate cancer cells. *Cancer Res*. 2006;66(19):9519–9*526*.
45. Carl-McGrath S, Lendeckel U, Ebert M, Roessner A, Röcken C. The disintegrin-metalloproteinases ADAM9, ADAM12, and ADAM15 are upregulated in gastric cancer. *Int J Oncol*. 2005;26(1):17–24.
46. O'Shea C, et al. Expression of ADAM-9 mRNA and protein in human breast cancer. *Int J Cancer*. 2003;105(6):754–761.
47. Grützmann R, et al. ADAM9 expression in pancreatic cancer is associated with tumour type and is a prognostic factor in ductal adenocarcinoma. *Br J Cancer*. 2004;90(5):1053–1058.
48. Abety AN, et al. Stromal fibroblast-specific expression of ADAM-9 modulates proliferation and apoptosis in melanoma cells in vitro and in vivo. *J Invest Dermatol*. 2012;132(10):2451–2458.
49. Grignani G, et al. Mechanisms of platelet activation by cultured human cancer cells and cells freshly isolated from tumor tissues. *Invasion Metastasis*. 1989;9(5):298–309.
50. McQuaid KR, Laine L. Systematic review and meta-analysis of adverse events of low-dose aspirin and clopidogrel in randomized controlled trials. *Am J Med*. 2006;119(8):624–638.
51. Rothwell PM, Wilson M, Price JF, Belch JF, Meade TW, Mehta Z. Effect of daily aspirin on risk of cancer metastasis: a study of incident cancers during randomised controlled trials. *Lancet*. 2012;379(9826):1591–1601.
52. Seshasai SR, et al. Effect of aspirin on vascular and nonvascular outcomes: meta-analysis of randomized controlled trials. *Arch Intern Med*. 2012;172(3):209–216.
53. Sostres C, Lanas A. Gastrointestinal effects of aspirin. *Nat Rev Gastroenterol Hepatol*. 2011;8(7):385–394.
54. Allegra M, et al. Rapid decay of alpha6 integrin caused by a mis-sense mutation in the propeller domain results in severe junctional epidermolysis bullosa with pyloric atresia. *J Invest Dermatol*. 2003;121(6):1336–1343.
55. Pulkkinen L, Kimonis VE, Xu Y, Spanou EN, McLean WH, Uitto J. Homozygous alpha6 integrin mutation in junctional epidermolysis bullosa with congenital duodenal atresia. *Hum Mol Genet*. 1997;6(5):669–674.
56. Waight JD, Hu Q, Miller A, Liu S, Abrams SI. Tumor-derived G-CSF facilitates neoplastic growth through a granulocytic myeloid-derived suppressor cell-dependent mechanism. *PLoS One*. 2011;6(11):e27690.
57. Cazenave JP, Ohlmann P, Cassel D, Eckly A, Hechler B, Gachet C. Preparation of washed platelet suspensions from human and rodent blood. *Methods Mol Biol*. 2004;272:13–28.
58. Perrault C, et al. A novel monoclonal antibody against the extracellular domain of GPIbbeta modulates vWF mediated platelet adhesion. *Thromb Haemost*. 2001;86(5):1238–1248.
59. Schaff M, et al. Novel function of tenascin-C, a matrix protein relevant to atherosclerosis, in platelet recruitment and activation under flow. *Arterioscler Thromb Vasc Biol*. 2011;31(1):117–124.
60. Mangin P, et al. Signaling role for phospholipase C gamma 2 in platelet glycoprotein Ib alpha calcium flux and cytoskeletal reorganization. Involvement of a pathway distinct from FcR gamma chain and Fc gamma RIIA. *J Biol Chem*. 2003;278(35):32880–32891.